An explanation for the missing EPR from the isolated substitutional gold impurity in silicon



1991 J. Phys.: Condens. Matter 3 4421

(http://iopscience.iop.org/0953-8984/3/24/012)

J. Phys.: Condens. Matter 3 (1991) 4421–4432. Printed in the UK

# An explanation for the missing EPR from the isolated substitutional gold impurity in silicon

Frederick G Anderson†

Institut Supérieur d'Electronique du Nord, 41 Boulevard Vauban, F-59046 Lille Cédex, France

Received 25 January 1991

**Abstract.** EPR from the isolated substitutional $Au^0$ impurity in silicon has never been observed, although EPR is seen for the isolated substitutional $Pt^-$ impurity in silicon, which is isoelectronic. The EPR of the $Pt^-$ defect shows $C_{2v}$ symmetry, a result of static Jahn–Teller distortions. Using a recently proposed vacancy-model-based electronic structure for $Pt^-$, we show that if the Pt impurity were tunnelling between the two trigonal distortions associated with a given tetragonal distortion, then $g_\perp$ would be nearly zero. We propose that the Au atom is tunnelling and that the tunnelling splitting is at least a few $cm^{-1}$. With such a tunnelling splitting and with $g_\perp$ nearly zero, under 'typical conditions', the EPR from the $Au^0$ defect would not be observed. We examine the effects of uniaxial stress. Finally, we show how it may be possible to observe EPR from this $Au^0$ defect in silicon.

## 1. Introduction

Considerable effort has been spent without success in trying to detect the electron paramagnetic resonance (EPR) of the neutral isolated substitutional gold impurity in silicon. By contrast, gold-related defects have been observed by EPR [1–3]. In addition, both donor and acceptor levels of a gold species in silicon, quite possibly the isolated substitutional gold impurity, have been observed by deep-level transient spectroscopy (DLTS) [4]. In contrast to this gold defect, the negatively charged isolated substitutional platinum impurity in silicon is easily observed by EPR, first by Woodbury and Ludwig [5]. Given that Au and Pt are neighbours on the periodic table of elements, and that $Au^0$ is isoelectronic to $Pt^-$, we expect that these two defects would behave very similarly. Hence, it is quite surprising that the $Pt^-$ defect is so readily observed while the $Au^0$ defect is so elusive.

The $Pt^-$ defect has been studied in depth with EPR [6]. From this study, a detailed model for the electronic structure of the $Pt^-$ defect was developed [7]. Since the $Au^0$ and $Pt^-$ defects are expected to behave similarly, we search in what we know about the $Pt^-$ defect for an explanation as to why the $Au^0$ defect has not yet been observed. The purpose of this work is to propose an explanation for the missing EPR from the $Au^0$ defect, based on the experimental results for the $Pt^-$ defect, and to suggest how the $Au^0$ defect may be observed.

† Present address: Department of Physics, Bldg 16, Lehigh University, Bethlehem, PA 18015, USA

0953-8984/91/244421+12$03.50  

We start by reviewing the model for the electronic structure of the $Pt^-$ defect. This may be considered as a (static) crystal-field model for the $Au^0$ defect. We then include dynamic effects, i.e. tunnelling. The inclusion of such effects is justified in the light of the experimental results for the $Pt^-$ defect. We show how these dynamic effects may render the $Au^0$ defect unobservable with EPR under what might be called 'typical conditions'. We then examine the effects of applying a uniaxial stress. Finally, we discuss our results, and suggest how the $Au^0$ defect might be observed with EPR.

## 2. Crystal-field model

The starting point for our model of the electronic structures of isolated substitutional impurities at the heavy end of the transition-metal series is the vacancy model proposed by Watkins [8]. In general, the electronic structure of a substitutional defect results from the interaction between the impurity's valence orbitals and the orbitals of the vacancy that the impurity atom fills. The vacancy model predicts that the defect-induced states lying in the band gap are those of a $t_2$ manifold and that these states possess a strong vacancy-like character, a result of the impurity d states, which lie deep within the valence band, interacting only weakly with vacancy-induced $t_2$ states, normally found in the band gap. The population of the $t_2$ gap manifold is determined by the number of impurity valence electrons and by the charge state of the defect. For both the $Au^0$ and $Pt^-$ defects, there will be three electrons in the $t_2$ gap manifold. Ten of the impurity valence electrons (all, in the case of Pt) completely fill the d states in the valence band. The neutral vacancy in silicon has two electrons in the $t_2$ gap manifold, the other two filling the $a_1$ state in the valence band that results from the creation of a vacancy. The extra electron to give the negative charge state for the $Pt^-$ defect, or in the case of $Au^0$ defect the remaining valence electron, is also found in the $t_2$ gap manifold. Hence, we expect these defects to be similar to the negative vacancy defect. This is the essence of the vacancy model.

The $C_{2v}$ symmetry of the negative vacancy is a result of two static Jahn–Teller distortions. The first is a tetragonal distortion that defines one of the cubic axes as the $z$-axis. The second is a trigonal distortion that involves the displacement of the impurity atom along either the positive or negative $z$-axis. We define a defect coordinate system as $x \sim [110]$, $y \sim [\bar{1}10]$, and $z \sim [001]$. The model for the $Pt^-$ defect given in [7] shows the splitting of the $t_2$ gap manifold by the Jahn–Teller effect to be that shown in figure 1 for that orientation of the defect having the neighbouring $^{29}Si$ hyperfine in the $xz$-plane. The coupling to the tetragonal distortion is found to be significantly stronger than the coupling to the trigonal distortion. We proceed by neglecting the presence of the $|z\rangle$, and focus our attention on the quadruplet $\{|x^+\rangle, |x^-\rangle, |y^+\rangle, |y^-\rangle\}$. The '+' and '−' denote the spin states 'up' and 'down', respectively. These four one-electron states are populated with three electrons. We define the many-electron state $|X^\sigma\rangle$ to be the Slater determinant $|(y^+y^-x^\sigma)\rangle$; the many-electron state $|Y^\sigma\rangle$ is defined to be the Slater determinant $|(x^+x^-y^\sigma)\rangle$.

The strength of the coupling to the trigonal distortion is found to be of the same size as the spin–orbit interaction. The Hamiltonian describing the splitting between $|X\rangle$ and $|Y\rangle$ arising from the trigonal distortion is

$$\mathcal{H}_{\text{trig}} = VQ(|X\rangle\langle X| - |Y\rangle\langle Y|) \tag{1}$$

where $V$ gives the Jahn–Teller coupling strength and $Q$ is the trigonal distortion coordinate. Associated with the trigonal distortion is a harmonic lattice potential

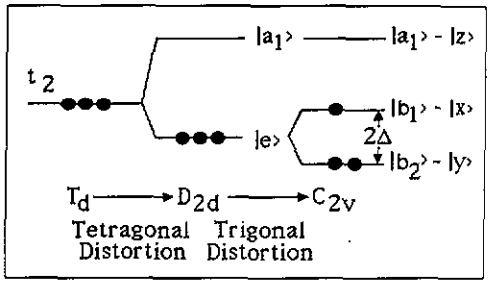


**Figure 1.** The splitting of the $t_2$ gap manifold by the two static Jahn–Teller distortions. The ordering of the states is for the defect orientation in which the $^{29}Si$ hyperfine is in the $xz$-plane.

energy, $\mathcal{H}_{pot} = (kQ^2/2)\mathbf{I}$, where $k$ is an effective spring constant, and $\mathbf{I}$ is the identity operator in electron space. The spin–orbit interaction is given by

$$\mathcal{H}_{so} = i\Gamma(|X^-\rangle\langle Y^-| - |Y^-\rangle\langle X^-| - |X^+\rangle\langle Y^+| + |Y^+\rangle\langle X^+|) \tag{2}$$

where $\Gamma = -N^2\xi_{Pt}/2$, $\xi_{Pt}$ is the platinum one-electron spin–orbit parameter, and $N^2$ gives the degree of localization of the $t_2$ orbitals on the platinum atom. Using the variational method of Öpik and Pryce [9], we find the states corresponding to the lowest energy configurations are

$$\begin{aligned} |\psi^+\rangle &= \cos\theta|X^+\rangle + i\sin\theta|Y^+\rangle \\ |\psi^-\rangle &= \cos\theta|X^-\rangle - i\sin\theta|Y^-\rangle \end{aligned} \tag{3}$$

where

$$\begin{aligned} \cos 2\theta &= \frac{VQ}{(V^2Q^2 + \Gamma^2)^{1/2}} \\ \sin 2\theta &= \frac{-\Gamma}{(V^2Q^2 + \Gamma^2)^{1/2}} \end{aligned} \tag{4}$$

and $VQ$ is either positive or negative, depending upon the sense of the trigonal distortion.

For simplicity, our consideration of the Zeeman interaction is restricted to the spin contribution alone $\mathcal{H}_Z = \beta g_e \boldsymbol{S}\cdot\boldsymbol{B}$. While the orbital contribution is important in a detailed study of the $Pt^-$ defect, for our purposes here we can neglect it, since its inclusion does not change our results qualitatively. The orbital contribution to the Zeeman interaction and the inclusion of the excited state $|z\rangle$ give rise to the (small) differences between the $g$ values that are measured in experiment and those found here in our simplified analysis. Within the $S = \frac{1}{2}$ manifold defined in equation (3), the $g$ values are

$$\begin{aligned} g_x &= g_y = g_e\cos 2\theta \\ g_z &= g_e. \end{aligned} \tag{5}$$

For the $Pt^-$ defect, in which $|VQ| \approx |\Gamma|$, $g_x = g_y \approx 1.42$, and $g_z = 2.00$. Given the crudeness of our approximations, we find surprisingly good agreement with the experimental values of $g_x = 1.3867$, $g_y = 1.4266$, and $g_z = 2.0789$.

We note the limiting values for the $g$ values given in equation (5). For the case in which the coupling to the trigonal distortion dominates the spin–orbit interaction ($|VQ| \gg |\Gamma|$), $|g_x|$ and $|g_y|$ approach the limiting value $g_e$. For the case in which the spin–orbit interaction dominates the coupling to the trigonal distortion ($|\Gamma| \gg |VQ|$), $g_x$ and $g_y$ approach the limiting value zero. This latter limit is reached in the case in which there is no trigonal distortion, in which case $|X\rangle$ and $|Y\rangle$ are degenerate.

In this section, we have presented a model for the electronic structure of the $Pt^-$ defect in silicon that explains the experimentally observed $g$ values. We expect that a static model for the electronic structure of the $Au^0$ defect would be similar to this model. We proceed under this assumption.

## 3. Tunnelling model

There are six equivalent distortions for the $Pt^-$ defect. These are divided into three pairs, each pair being associated with a tetragonal distortion along one of the cubic axes. The pair of equivalent distortions associated with a given tetragonal distortion arises from the two possible senses of the trigonal distortion ($Q > 0$ or $Q < 0$) corresponding to the two possibles senses of the impurity atom displacement along the $z$-axis. The distortion for which $VQ > 0$, we label $A$; the distortion for which $VQ < 0$, we label $B$. From equations (4) and (5), we see that changing the sign of $VQ$ (changing the sense of the trigonal distortion) has the effect of changing the sign of $g_x$ and $g_y$. So, $g_x(VQ) = -g_x(-VQ)$, and similarly for $g_y$. $g_z$ is unaffected by the sense of the trigonal distortion.

Experiments involving uniaxial stress showed one particularly interesting result for the $Pt^-$ defect: Even at temperatures as low as 2 K, the $Pt^-$ defect reorients when uniaxial stress is either applied or removed [6]. In the presence of uniaxial stress, the equivalence between the various distortions is broken, i.e. certain distortions are more energetically favourable than others. That this reorientation occurs at such low temperatures suggests that the defect is tunnelling from one distortion to another. The timescale for this tunnelling is observed to be at the most of the order of seconds. However, since an EPR spectrum that clearly shows a static distortion is observed, the reorientation rate must be slower than the linewidths [10]; that is the $Pt^-$ defect is continuously reorienting between the six equivalent distortions, but this reorientation is slow enough such that the defect remains within a given distortion long enough to show an EPR spectrum with sharp lines corresponding to a defect in a lower symmetry configuration. We continue by considering the mechanism that drives the tunnelling between the distortions $A$ and $B$, and what the consequences are if the tunnelling rate between these two senses of the trigonal distortion is increased.

In the static model of the previous section, we neglected the vibrations of the lattice, and in particular the lattice vibrations of the same symmetry as the trigonal distortion. These trigonal modes of vibration are centred on the trigonal distortions, i.e. there are trigonal vibrations about the distortions $A$ and $B$. The zero-point vibrational state centred on the distortion $A$ we denote by $|A\rangle$; that centred on $B$, we denote by $|B\rangle$. We create *vibronic* states that are simple Born–Oppenheimer products of electronic and vibrational states. The vibronic states $|\Psi_A^+\rangle$ and $|\Psi_A^-\rangle$ are defined by

$$|\Psi_A^{+(-)}\rangle = |\psi_A^{+(-)}\rangle|A\rangle \tag{6}$$

and similarly for $|\Psi_B^{+(-)}\rangle$.

The kinetic energy operator for the vibrations is $\mathcal{H}_{\rm kin} = (P^2/2M)\mathbf{I}$, where $P$ is the momentum conjugate to the trigonal distortion coordinate $Q$, and $M$ is the effective mass for the trigonal mode of vibration. In the absence of the spin–orbit interaction $|\Psi_A^{+(-)}\rangle = |Y^{+(-)}\rangle$ and $|\Psi_B^{+(-)}\rangle = |X^{+(-)}\rangle$. Hence the matrix elements of the vibrational kinetic energy operator vanish when taken between the vibronic states localized in the two distortions. However, with the spin–orbit interaction included, the electronic states within the vibronic states are combinations of $|X\rangle$ and $|Y\rangle$; so, the matrix elements of the vibrational kinetic energy between the two distortions are non-vanishing. We find

$$\begin{aligned}\langle\Psi_B^{+(-)}|\mathcal{H}_{\rm kin}|\Psi_A^{+(-)}\rangle &= \langle B|P^2/2M|A\rangle \sin 2\theta \\ &\equiv T\sin 2\theta.\end{aligned} \tag{7}$$

This equation shows that the vibrational kinetic energy of the trigonal modes mixes the vibronic states centred on the distortions $A$ and $B$. Hence, it is the vibrational kinetic energy of the trigonal modes that drives the tunnelling between the two distortions.

The interdistortion matrix elements mix the vibronic states associated with the two distortions. The two vibronic doublets given by equations (3) and (6) are degenerate. The mixing of these doublets, i.e. the inclusion of tunnelling, gives rise to a tunnelling splitting, $2E_{\rm T}$, that removes this degeneracy as shown in figure 2. The resulting tunnelling states are

$$\begin{aligned}|\Phi_L^{+(-)}\rangle &= N_L(\cos\gamma|\Psi_A^{+(-)}\rangle - \mathrm{sgn}(\Gamma)\sin\gamma|\Psi_B^{+(-)}\rangle) \\ |\Phi_H^{+(-)}\rangle &= N_H(\mathrm{sgn}(\Gamma)\sin\gamma|\Psi_A^{+(-)}\rangle + \cos\gamma|\Psi_B^{+(-)}\rangle)\end{aligned} \tag{8}$$

where

$$\mathrm{sgn}(x) = \begin{cases} +1 & \text{if } x > 0 \\ -1 & \text{if } x < 0 \end{cases} \tag{9}$$

and $\gamma = -\pi/4$. $N_{L(H)}$ are normalization constants.

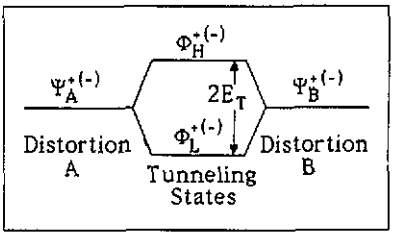


**Figure 2.** The vibronic doublets $|\Psi_A^{+(-)}\rangle$ and $|\Psi_B^{+(-)}\rangle$ are the states found in the static crystal-field model for the two senses of trigonal distortion. These states are mixed by the kinetic energy of the trigonal mode vibrations. This mixing gives rise to the tunnelling states $|\Phi_L^{+(-)}\rangle$ and $|\Phi_H^{+(-)}\rangle$ that are split by an energy of $2E_{\rm T}$, the tunnelling splitting.

The tunnelling splitting increases as the strength of the Jahn–Teller coupling decreases. The limit in which $E_{\rm T} = 0$ corresponds to the case in which there is absolutely

no tunnelling between the two distortions, the purely static limit of Jahn–Teller coupling. In the case of the $Pt^-$ defect, $E_T$ is almost, but not identically, zero. Although there is tunnelling between the two distortions, the tunnelling rate, $\nu = 2E_T/h$, is slow compared with the EPR linewidth. Hence, an EPR spectrum showing a statically distorted defect is observed. In the limit in which there is no Jahn–Teller coupling to the trigonal distortions, the doublet splitting is simply that resulting from the spin–orbit interaction, i.e. $E_T = \Gamma$.

We now consider the Zeeman interaction within the states given in equation (8). As before, we consider only the spin contribution to the Zeeman interaction. The non-zero matrix elements are

$$\langle \Phi_L^+ | \mathcal{H}_Z | \Phi_L^+ \rangle = -\langle \Phi_L^- | \mathcal{H}_Z | \Phi_L^- \rangle = \beta g_e B_z/2 \tag{10a}$$

$$\langle \Phi_H^+ | \mathcal{H}_Z | \Phi_H^+ \rangle = -\langle \Phi_H^- | \mathcal{H}_Z | \Phi_H^- \rangle = \beta g_e B_z/2 \tag{10b}$$

$$\langle \Phi_H^+ | \mathcal{H}_Z | \Phi_L^+ \rangle = -\langle \Phi_H^- | \mathcal{H}_Z | \Phi_L^- \rangle = N_H N_L \langle A|B \rangle \cos 2\gamma \sin 2\theta \beta g_e B_z/2 \tag{10c}$$

$$\langle \Phi_L^- | \mathcal{H}_Z | \Phi_L^+ \rangle = N_L^2 \cos 2\theta_A \cos 2\gamma \beta g_e (B_x + iB_y)/2 \tag{10d}$$

$$\langle \Phi_H^- | \mathcal{H}_Z | \Phi_H^+ \rangle = N_H^2 \cos 2\theta_B \cos 2\gamma \beta g_e (B_x + iB_y)/2 \tag{10e}$$

$$\langle \Phi_L^- | \mathcal{H}_Z | \Phi_H^+ \rangle = \langle \Phi_H^- | \mathcal{H}_Z | \Phi_L^+ \rangle = N_L N_H \mathrm{sgn}(\Gamma) \cos 2\theta_A \beta g_e (B_x + iB_y)/2. \tag{10f}$$

For $\gamma = -\pi/4$, the right-hand side of equations (10*c*), (10*d*), and (10*e*) are zero. In figure 3, we plot the qualitative splitting of the tunnelling states in the presence of magnetic fields in the $z$- and $x$-directions.

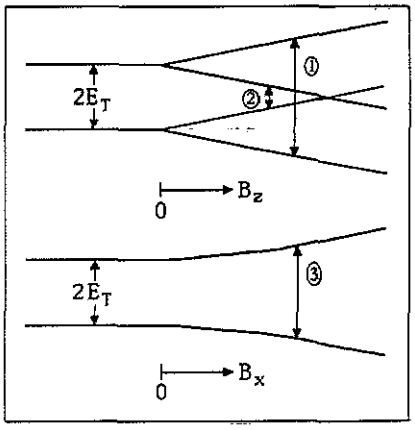


**Figure 3.** The qualitative magnetic field splitting of the tunnelling states in the presence of (*a*) a magnetic field along the $z$-axis; and (*b*) a magnetic field along the $x$-axis. The allowed EPR (magnetic-dipole) transitions are shown by the full vertical arrows.

The transitions occurring in EPR are magnetic-dipole transitions. Hence, the allowed transitions can be determined from the matrix elements given in equation (10), where $\boldsymbol{B}$ is now the magnetic field associated with the microwaves used to induce the spin flips. The allowed magnetic-dipole transitions are marked in figure 3.

Using figure 3, we can determine the resulting EPR spectrum. The energy required to make the spin flips marked '1' and '3' in the figure are greater than $2E_T$. For $\nu_{micro} = 20$ GHz, where $\nu_{micro}$ is the microwave frequency, we find that $h\nu_{micro} \simeq 0.7$ cm$^{-1}$. Hence, even for tunnelling splittings that are small, $2E_T \simeq 1$ cm$^{-1}$, it is not possible to make these transitions, i.e. no EPR will be observed!

The spin flip marked '2' in the figure is possible for any microwave frequency, assuming that the applied magnetic field is large enough to sufficiently reduce the energy splitting between the two states involved. Even for applied fields of 4 T and $\nu_{micro} = 20$ GHz, if $2E_T > 4$ cm$^{-1}$ it is not possible to make this spin flip.

In the case of the $Pt^-$ defect, $E_T$ is nearly zero; and so an EPR spectrum showing a $C_{2V}$ distortion is observed. However, in light of the low temperature reorientation observed with the $Pt^-$ defect, we propose that the $Au^0$ defect could quite possibly be so dynamic that the tunnelling splitting is large enough such that under 'typical conditions', no EPR will be observed.

## 4. Effects of uniaxial stress

The very general idea that the $Au^0$ defect in silicon is dynamic and that somehow this property is responsible for the missing EPR from this defect is not new, though up to now a detailed explanation has not been proposed. It seems natural that the application of stress may force this defect into a particular static configuration, and therefore allow the detection of EPR. Hence, we examine the effects of stress within our model. In particular, we consider uniaxial stress along a ⟨110⟩ direction (in the cubic axis system) that is perpendicular to the tetragonal distortion. Such a stress has the effect of destroying the equivalence between the distortions $A$ and $B$, i.e. the vibronic doublets $|\Psi_A^{+(-)}\rangle$ and $|\Psi_B^{+(-)}\rangle$ are no longer degenerate, as seen by the coupling between the electronic states and this ⟨110⟩ stress,

$$\mathcal{H}_S = V_2\sigma_{110}(|X\rangle\langle X| - |Y\rangle\langle Y|) \tag{11}$$

where $\sigma_{110}$ is the size of the stress and $V_2$ is the strength of the coupling. When the vibronic doublets are degenerate, the mixing of these vibronic doublets in the tunnelling doublets will be in equal proportions. This balance results in the value of $-\pi/4$ for $\gamma$, ultimately to the result that the only allowed magnetic-dipole transitions are *between* the tunnelling doublets. Breaking the equivalence between these two distortions, e.g. through the presence of a uniaxial ⟨110⟩ stress, results in an unbalanced mixing of the vibronic doublets in the tunnelling doublets, and should then lead to the observation of EPR. In the presence of this ⟨110⟩ stress, the tunnelling states are still given by equation (8), but now

$$\gamma = \tan^{-1}\left[\frac{V_2\sigma_{110}\cos 2\theta_B - [V_2^2\sigma_{110}^2\cos^2 2\theta_B + T^2\sin^2 2\theta_B]^{1/2}}{|T\sin 2\theta_B|}\right] \tag{12}$$

$N_{L(H)}$ are still normalization constants, though their values have changed from their values in the absence of stress.

We now consider the matrix elements of the Zeeman interaction with these new tunnelling states. The non-zero matrix elements are those given in equation (10), where the right-hand sides of equations (10*c*), (10*d*) and (10*e*) are no longer zero.

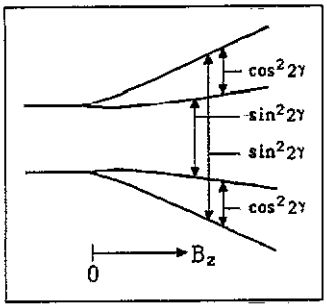


**Figure 4.** The qualitative magnetic field splitting in the presence of a ⟨110⟩ uniaxial stress of the tunnelling states for a magnetic field along the $z$-axis. The allowed EPR transitions, with their relative intensities, are shown by the full vertical arrows.

Figure 4 shows the qualitative magnetic field splitting in the presence of a ⟨110⟩ uniaxial stress for a field along the $z$-direction. We note that as a result of the matrix elements given by equation (10$c$), these magnetic field splittings are no longer linear.

Also shown in figure 4 are the allowed EPR transitions with their relative intensities. The transitions with intensity $\sin^2(2\gamma)$ are just those marked '1' and '3' in figure 3. Hence, as before, the microwave photon energy and the size of the applied magnetic field may not be sufficient to effect these transitions. We also note that this transition energy is a function of $\gamma$, through the matrix elements of equation (10$c$). Hence, the $g$ value will be a function of stress. The stress-induced transitions have a relative intensity of $\cos^2(2\gamma)$ and occur *within* each of the tunnelling doublets. These transitions will have a $g$ value (neglecting orbital effects) of $g_z = g_e$. Hence, the presence of a ⟨110⟩ uniaxial stress gives rise to EPR that is observable under 'typical conditions'.

When a ⟨110⟩ stress is applied, a magnetic field along the $x$- or $y$-axis will split each of the tunnelling doublets. From the $\cos(2\gamma)$ factor in equations (10$d$) and (10$e$), however, the $g_x$ and $g_y$ will be functions of stress.

We consider briefly the effects of uniaxial stress along the cubic-axis directions. Uniaxial ⟨001⟩ stress parallel to the tetragonal distortion shifts by equal amounts and in the same sense each of the vibronic doublets $|\Psi_A^{+(-)}\rangle$ and $|\Psi_B^{+(-)}\rangle$. This stress also contributes to the mixing of these two doublets. Uniaxial ⟨100⟩ stress perpendicular to the tetragonal distortion also shifts by equal amounts the two vibronic doublets, but in the opposite sense to the case of the stress parallel to the tetragonal distortion. In addition, the uniaxial ⟨100⟩ stress contributes to the mixing of the doublets. Hence, uniaxial stress along the cubic-axis directions does not remove the equivalence between the two distortions.

Finally, we consider the effects of random strains in the crystal [11]. The random strains act in the same way as uniaxial stress; so, random strains can lift the degeneracy between the two vibronic doublets $|\Psi_A^{+(-)}\rangle$ and $|\Psi_B^{+(-)}\rangle$. If the strain-induced splitting between the two vibronic doublets is small compared to the tunnelling splitting, the effect of the random strains is simply to broaden the EPR lines, through the strain dependence ($\gamma$) of the $g$ values, making the EPR more difficult to observe. This broadening is also found for $g_z$ where the orbital contribution to the Zeeman

interaction, given by

$$\begin{aligned}\langle\Phi^{+}_{L(H)}|\beta L_z B_z|\Phi^{+}_{L(H)}\rangle &= -\langle\Phi^{-}_{L(H)}|\beta L_z B_z|\Phi^{-}_{L(H)}\rangle \\ &= N^2_{L(H)}N^2\sin 2\theta + (-)\sin 2\gamma\langle A|B\rangle\end{aligned} \tag{13}$$

is a function of $\gamma$.

For the case in which the strain-induced splitting between the vibronic doublets is comparable with or greater than the tunnelling splitting, the random strains themselves should give rise to observable EPR. However, phonon-induced motional averaging between the two senses of the trigonal distortion may again render the $Au^0$ defect unobservable in EPR.

## 5. Discussion

In the absence of a trigonal distortion, the spin–orbit interaction creates two Kramers doublets from the orbital doublet $\{|X\rangle, |Y\rangle\}$. Within each of these two Kramers doublets, the matrix elements of the spin contribution to the Zeeman interaction are zero for the case when the magnetic field is perpendicular to the $z$-axis, which is defined by the tetragonal distortion. These vanishing matrix elements account for two results. The first is that $g_x$ and $g_y$ are both zero. The second is that, although a magnetic field $B_z$ will split each of the Kramers doublets, the magnetic-dipole transitions between the two states belonging to a given Kramers doublet are forbidden, since there is no coupling to magnetic fields perpendicular to the $z$-axis. The net effect of these two results is that EPR will not be observed.

We note that it is possible for the spin–orbit interaction to stabilize a system against a Jahn–Teller distortion: that is if the strength of the spin–orbit interaction is strong enough, there would be no Jahn–Teller distortion. For the case of the $Pt^-$ defect, the strength of the spin–orbit interaction is approximately the same size as the strength of the Jahn–Teller coupling involving the trigonal distortion. So, another possible explanation for the missing EPR from the $Au^0$ defect is that the spin–orbit interaction stabilizes this defect against a trigonal Jahn–Teller distortion. Hence, as described in the previous paragraph, no EPR will be observed. This explanation, however, requires that the differences between the $Au^0$ and $Pt^-$ defects are more severe than for the explanation based on the tunnelling model that we have described.

The trigonal distortion lifts the degeneracy of the orbital doublet, i.e. the equivalence between $x$ and $y$ is broken. Hence, the Kramers doublets created by the spin–orbit interaction no longer possess an equal balance of the states $|X\rangle$ and $|Y\rangle$ needed to achieve the cancellation that results in $g_x$ and $g_y$ both being zero. Therefore, magnetic fields perpendicular to the $z$-axis will split the Kramers doublets, and transitions between the two states belonging to a given Kramers doublet that is split by a magnetic field $B_z$ become allowed. Hence, EPR will be observed.

The trigonal distortion has two senses ($Q > 0$ and $Q < 0$), which give rise to two equivalent distorted defects ($A$ and $B$). Since these two distortions are energetically equivalent, the vibronic states associated with these two distortions ($|\Psi^{+(-)}_A\rangle$ and $|\Psi^{+(-)}_B\rangle$) are degenerate. Hence, when these vibronic states are mixed by the kinetic energy of the trigonal mode vibrations, the resulting tunnelling doublets are very similar in form to the Kramers doublets that are found in the case when there

is no trigonal distortion. The tunnelling doublets $|\Phi_L^{+(-)}\rangle$ and $|\Phi_H^{+(-)}\rangle$ describe the tunnelling between the two senses of the trigonal distortion. As is the case for the Kramers doublets, the matrix elements of the spin contribution to the Zeeman interaction within each of the tunnelling doublets are zero for the case of the magnetic field being perpendicular to the $z$-axis. Hence, no EPR corresponding to transitions within each of the tunnelling doublets will be observed. The only allowed magnetic-dipole transitions occur between the two tunnelling doublets. For the case of the $Pt^-$ defect, the tunnelling rate is slow enough, i.e. the tunnelling splitting is so small, that the two tunnelling doublets are essentially degenerate. This is the static limit of the Jahn–Teller coupling and the observed EPR is simply that predicted by the static crystal-field model. We are proposing that for the $Au^0$ defect, the tunnelling splitting between the two tunnelling doublets is larger, i.e. the tunnelling rate is faster, and that the tunnelling splitting is large enough such that the $Au^0$ defect will not be observed in EPR.

We can easily understand how the $g_x$ and $g_y$ become zero when tunnelling is included. We recall from the static crystal-field model that $g_x$ and $g_y$ for the two senses of the trigonal distortion had the same magnitudes but opposite signs. When the system tunnels from one distortion to the other, an average of the two values is obtained; and the average of $g_x$ and $g_y$ for the two senses of distortion is zero. This average is zero only when the vibronic states associated with the two distortions are degenerate.

The most direct method to observe via some kind of EPR the $Au^0$ defect is to use microwaves whose photon energy is greater than the tunnelling splitting or high frequency microwaves in conjunction with very large magnetic fields. Unfortunately, an accurate estimate for the tunnelling splitting is not available. The range of possible values covers two orders of magnitude, from 1 to 100 $cm^{-1}$. As the $Pt^-$ defect has an approximately vanishing tunnelling splitting, we might expect the tunnelling splitting for the $Au^0$ defect to be of the order of 10 $cm^{-1}$.

We have demonstrated how the trigonal distortion lifts the degeneracy between the $|X\rangle$ and $|Y\rangle$ states and gives rise to non-zero values for $g_x$ and $g_y$ within each of the vibronic doublets $|\Psi_A^{+(-)}\rangle$ and $|\Psi_B^{+(-)}\rangle$. Similarly, by removing the equivalence between the two senses of the trigonal distortion, we can find non-zero values for $g_x$ and $g_y$ within each of the tunnelling doublets $|\Phi_A^{+(-)}\rangle$ and $|\Phi_B^{+(-)}\rangle$. This is the effect of a $\langle 110\rangle$ uniaxial stress perpendicular to the $z$-axis. In the presence of such a stress, the distortions $A$ and $B$ are no longer equivalent. Hence, the tunnelling states are no longer constructed from equal amounts of the vibronic states associated with each distortion. So, the weighted averages of the $g_x$ and $g_y$ associated with each distortion are no longer zero. This allows magnetic-dipole transitions to occur within each of the tunnelling doublets. These transitions can be effected under 'typical conditions'.

The intensities of these transitions are dependent upon the size of the stress, larger stresses giving rise to stronger EPR intensities. Hence, EPR from the $Au^0$ defect might possibly be observed by applying a $\langle 110\rangle$ uniaxial stress. However, the presence of random strains would broaden these resonances making them harder to observe. On the other hand, larger random strains can play the role of uniaxial stress and give rise to observable EPR.

There are several factors that may inhibit the observation of EPR in the presence of $\langle 110\rangle$ uniaxial stress or random strains. The first is that the stress (strain) must be large enough such that the energy splitting between the two vibronic doublets is large

enough relative to the tunnelling splitting to give rise to a significantly intense transition. The second factor inhibiting the observation of EPR involves the reorientation of the defect. The ⟨110⟩ uniaxial stress-induced reorientation for the $Pt^-$ defect is observed to be such that, with compressional stress, there are fewer defects with their $z$-axis perpendicular to the direction of the stress, i.e. there are fewer defects properly aligned for observation. (In contrast to this, a tensile ⟨110⟩ stress would align more defects in the proper sense for observation.) Finally, even in the case of large random strains, motional averaging may again lead to $g_x$ and $g_y$ being nearly zero. These factors may explain why even under stress, the $Au^0$ defect has never been observed in EPR.

## 6. Conclusions

We have presented a model of the electronic structure of the isolated substitutional $Pt^-$ impurity in silicon, and have seen how even with our crude approximations we can explain quite accurately the experimentally observed $g$ values. We expect the isolated substitutional $Au^0$ impurity in silicon, which is isoelectronic to the $Pt^-$ defect, to have an electronic structure quite similar to that of the $Pt^-$ defect. However, in stark contrast to the $Pt^-$ defect, the $Au^0$ defect has never been observed in EPR. Using the electronic structure of the $Pt^-$ defect, we have proposed an explanation for this missing EPR. We propose that the tunnelling rate between the two senses of the trigonal distortion for the $Au^0$ defect is faster than that for the $Pt^-$ defect. Based on the experimentally observed low-temperature reorientation of the $Pt^-$ defect under stress, this hypothesis concerning the tunnelling rate of the $Au^0$ seems quite reasonable. We have shown how this tunnelling may account for the missing EPR from the $Au^0$ defect. In addition, we have shown how this same result can be reached if the spin–orbit interaction stabilizes this defect against trigonal distortions. While a ⟨110⟩ compressional uniaxial stress or random strains could lead to the observation of EPR from the $Au^0$ defect, we have described how this defect may remain unobservable in EPR.

EPR might be observed by applying a tensile ⟨110⟩ uniaxial stress or by using 'non-typical' microwave frequencies and magnetic fields.

## Acknowledgments

The author would like to thank M Lannoo and particularly F S Ham for their critical reading of this manuscript and their helpful suggestions.

## References

[1] Ludwig G W and Woodbury H H 1962 *Solid State Physics* vol 13, ed F Seitz and D Turnbull (New York: Academic) p 223

[2] Höhne M 1980 *Phys. Status Solidi* (b) 99 651
Kleinhenz R L, Lee Y H, Corbett J W, Sieverts E G, Müller S H and Ammerlaan C A J 1981 *Phys. Status Solidi* (b) 108 363

[3] Höhne M 1982 *Phys. Status Solidi* (b) 109 525

[4] Lang D V, Grimmeiss H G, Meijer E and Jaros M 1980 *Phys. Rev.* B 22 3917

Utzig J and Schröter W 1984 *Appl. Phys. Lett.* **45** 761
[5] Woodbury H H and Ludwig G W 1962 *Phys. Rev.* **126** 466
[6] Anderson F G, Milligan R F and Watkins G D *Phys. Rev.* submitted
[7] Anderson F G, Delerue C, Allan G and Lannoo M *Phys. Rev.* submitted
Anderson F G, Ham F S and Watkins G D *Phys. Rev.* submitted
[8] Watkins G D 1983 *Physica* B **117 &** 118 9
[9] Öpik U and Pryce M H L 1957 *Proc. R. Soc. London* A **238** 425
[10] Gurtowsky H S and Saika A 1953 *J. Chem. Phys.* **21** 1688
[11] Ham F S 1972 *Electron Paramagnetic Resonance* ed S Geschwind (New York: Plenum) p 1